Acta Astronautica 144 (2018) 297–304

Contents lists available at ScienceDirect

Acta Astronautica

journal homepage: www.elsevier.com/locate/actaastro

Plasma brake model for preliminary mission analysis

Leonardo Orsini, Lorenzo Niccolai *, Giovanni Mengali, Alessandro A. Quarta

Department of Civil and Industrial Engineering, University of Pisa, I-56122, Italy

ARTICLE INFO

Keywords:
Plasma brake
Coulomb drag
Preliminary mission design

ABSTRACT

Plasma brake is an innovative propellantless propulsion system concept that exploits the Coulomb collisions between a charged tether and the ions in the surrounding environment (typically, the ionosphere) to generate an electrostatic force orthogonal to the tether direction. Previous studies on the plasma brake effect have emphasized the existence of a number of different parameters necessary to obtain an accurate description of the propulsive acceleration from a physical viewpoint. The aim of this work is to discuss an analytical model capable of estimating, with the accuracy required by a preliminary mission analysis, the performance of a spacecraft equipped with a plasma brake in a (near-circular) low Earth orbit. The simplified mathematical model is first validated through numerical simulations, and is then used to evaluate the plasma brake performance in some typical mission scenarios, in order to quantify the influence of the system parameters on the mission performance index.

1. Introduction

The plasma brake [1,2] is an innovative technology capable of supplying a propulsive acceleration to a spacecraft on a low Earth orbit (LEO) without any propellant consumption, by exploiting the (electrostatic) Coulomb collisions between a long space tether and the charged particles in a plasma stream. In a typical configuration [2–4] a single charged tether deployed by a spacecraft, see Fig. 1, interacts with the ionized upper stages of Earth's atmosphere (ionosphere), and provides a decelerating thrust (Coulomb drag) orthogonal to the tether line.

The idea of plasma brake is a consequence of the Electric Solar Wind Sail (E-sail) propulsive concept, which can be traced back to 2004 [5]. This propulsion system consists of a spinning grid of tethers, stretched out by centrifugal force, which are kept at a high potential to exchange momentum with the solar wind ions and generate a small (but continuous) propulsive acceleration without any propellant consumption [6,7]. An E-sail-based spacecraft is a good candidate for some special heliocentric mission scenarios that would be difficult or impossible to achieve with a conventional propulsion system, including displaced non-Keplerian orbits [8,9], outer Solar System exploration [10], asteroids deflection [11], near-Earth asteroid flyby [12] or sample return mission [13].

The hypothesized structure of a plasma brake tether was originally based on the Hoytether [14] concept, in which the tether has some primary lines, with multiple interconnections made of smaller wires. This design provides a significant safety improvement against impacts with micrometeorids, thus increasing the system lifetime with respect to a single line tether. A more recent innovation in the field of space tether manufacturing is the Heytether [15], which is made of a single primary line with multiple secondary connections. Its structure guarantees a sufficient reliability, with a reduction of total mass and design complexity when compared to the Hoytether. In this context, a 1km-long Heytether has been obtained as one of the final outcomes of the European project EU FP7 [15–17], in view of future space tests of the E-sail technology.

A first validation test for a plasma brake (and E-sail) system was tried in 2013 by the Estonian satellite ESTCube-1 [18,19], but a failure occurred to the tether reel mechanism, probably due to the vibrational loads during the launch phase. A second technology demonstration-spacecraft, the Finnish satellite Aalto-1 [20], should be launched during 2017. The Aalto-1 is a 3U CubeSat equipped with a 100m-long electrostatically charged tether, stretched out with the centrifugal force generated by spinning the satellite [21]. A plasma brake in-situ experiment will be conducted, both for positive and negative polarity of the tether, to obtain experimental evidence of the propulsion system concept. Another plasma brake experiment is planned by the more advanced ESTCube-2 satellite [22], which will carry a 300m-long tether. The spacecraft systems are currently under development and the launch readiness tests should be completed within 2018.

Some preliminary numerical simulations have been conducted to investigate the potential performance of a plasma brake system [4,23], with encouraging results in a classical deorbiting mission scenario. In this context, simulations give decaying times of few years for near or

* Corresponding author.
E-mail addresses: orsini.elle@libero.it (L. Orsini), lorenzo.niccolai@ing.unipi.it (L. Niccolai), g.mengali@ing.unipi.it (G. Mengali), a.quarta@ing.unipi.it (A.A. Quarta).

https://doi.org/10.1016/j.actaastro.2017.12.048
Received 7 March 2017; Received in revised form 5 May 2017; Accepted 31 December 2017
Available online 4 January 2018

Nomenclature

A	spacecraft frontal area, [m^2]
a	semimajor axis of the spacecraft osculating orbit, [km]
b_t	tether width, [cm]
C_D	drag coefficient
c_b	ballistic coefficient, [kg/m^2]
e	elementary charge, [C]
F	magnitude of plasma brake-induced drag, [mN]
f_i	auxiliary functions, see Eqs. (6)–(8)
g_0	standard gravity, [m/s^2]
h	spacecraft altitude, [km]
h_0	spacecraft initial altitude, [km]
K	plasma brake constant, see Eq. (1)
k_B	Boltzmann constant, [J/K]
L_t	tether length, [m]
m_0	spacecraft initial mass, [kg]
m_i	mean molecular mass of the incoming flow, [u]
m_L	payload mass, [kg]
m_{rm}	tether reel mechanism mass, [kg]
m_{sav}	fraction of mass saving
n_0	plasma bulk number density, [m^{-3}]
$R_\oplus$	Earth's radius, [km]
r_w	wire radius, [μm]
T	temperature of ions, [K]
V_r	modified voltage, see Eq. (2) [V]
V_t	tether voltage, [V]
v_0	plasma bulk relative velocity, [km/s]
ε_0	vacuum dielectric constant, [F/m]
η_r	packaging factor of the reeled tether
λ	payload ratio
ρ_r	density of the reel structure with respect to the internal volume, [kg/m^3]
ρ_w	density of the wires material, [kg/m^3]
σ_S	thruster structural coefficient, [kg/m]
σ_t	tether structural coefficient, [mg/m]

Subscripts

C	chemical or electric thruster
i	generic part of the spacecraft
PB	plasma brake
SC	spacecraft
t	tether
w	wire

Superscripts

$\sim$	reference value
$-$	mean value

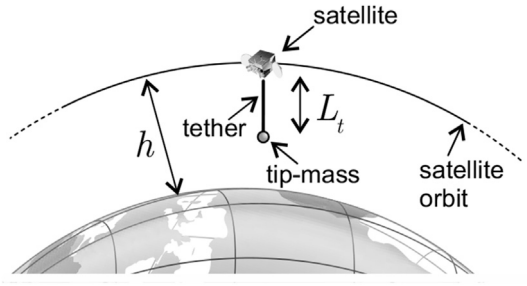

Fig. 1. Plasma brake conceptual scheme, adapted from Ref. [2].

mid-term tether lengths, and significant mass savings with respect to active deorbiting strategies with chemical or electric thrusters. For example, according to Ref. [4], a 5km-long tether produces a decelerating drag of 0.43mN at an altitude of 800km. This braking force is able to reduce the altitude of a 260kg spacecraft of about 100km in 1year. Based on previous technology developments [15–17], a tether length of 5km is estimated to be ready within the next 5 years.

The available mathematical models for plasma brake are however quite complex and depend on many different parameters, and a thorough analysis of its actual potentialities is not yet available. Therefore, the aim of this paper is to illustrate an analytical model capable of predicting the mission performance of a gravity gradient-stabilized spacecraft equipped with a plasma brake tether, with small computational costs compared to a simulative approach.

This paper is organized as follows. Section 2 presents an approximate mathematical model, based on some simplifying assumptions, which can be used to estimate the plasma brake-induced force by means of analytical formulas. The approximate model is then validated by simulation with a more general model in which the equations of motions are integrated numerically. Section 3 analyzes the plasma brake performance in a typical mission scenario as, for example, a deorbiting strategy. Finally, Section 4 contains some concluding remarks.

2. Approximate thrust model

Previous works [1,3,24] on plasma brake system analysis have shown that a negatively-charged tether is more convenient compared to a positively-charged one in terms of design simplicity, for a LEO mission scenario. In fact, in the positive polarity case, the plasma brake system requires a voltage source and an electron gun to maintain the necessary voltage by expelling the accumulated electrons. On the contrary, when the tether is negatively-charged, although the voltage source is still required, the ion gun (which is theoretically needed to keep the tether at the design voltage) is not essential for a proper system operation, since the spacecraft itself acts as an electron collector due to the high thermal mobility of electrons. Hence, only the negatively-charged tether case will be addressed in this paper. As the spacecraft is used as an electron collector, a part of the vehicle is electrically connected to the negatively biased tether. This arrangement poses additional constraints to the spacecraft system design as, for example, the fact that some components must be properly shielded with electric insulators.

Consider a spacecraft orbiting a LEO that at a certain time instant releases a single charged tether (with a tip mass) to generate a Coulomb drag, see Fig. 1. The spacecraft-tether-mass system is stabilized by gravity gradient, with the tether axis pointing towards the Earth's center-of-mass. According to Refs. [3,22], the thrust per unit length dl of a single negatively-charged tether can be expressed as

$$\frac{dF}{dl} = K\, m_i\, n_0\, v_0^2 \sqrt{\frac{\varepsilon_0\, V_r}{e\, n_0}} \exp\left(-\frac{m_i\, v_0^2}{2\, e\, V_r} \right) \tag{1}$$

where F is the magnitude of the plasma brake-induced drag force, m_i is the mean molecular mass of the incoming flow, n_0 and v_0 are the plasma bulk number density and the component of the plasma relative velocity (with respect to the tether) orthogonal to the tether axis, e is the elementary charge, ε_0 is the vacuum dielectric constant, and $K = 3.864$ is a dimensionless constant [3]. The term V_r in Eq. (1) is a sort of modified tether voltage [4] given by

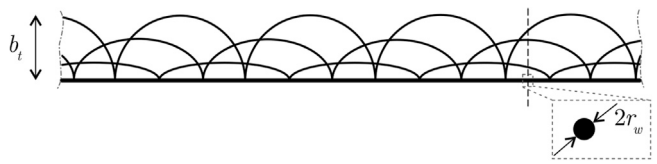

Fig. 2. Schematic representation of the four-wire Heytether (adapted from Ref. [33]).

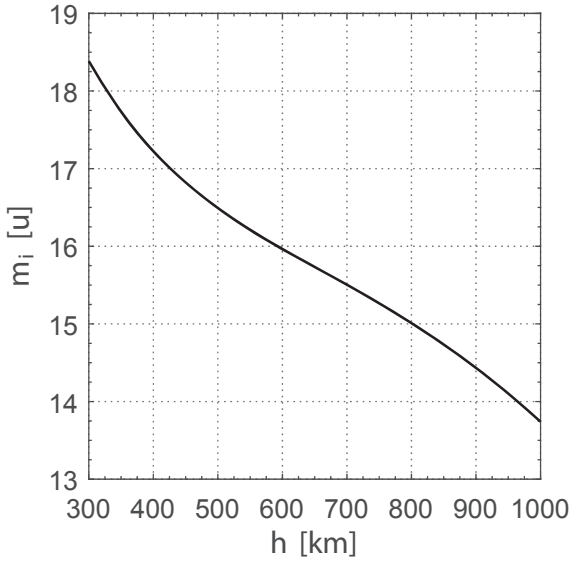

Fig. 3. Mean molecular mass of ions as a function of altitude for a mean solar activity.

$$V_r \triangleq \frac{2|V_t|}{\ln\left(\frac{\varepsilon_0 |V_t|}{e\, n_0\, b_t\, r_w}\right)} \tag{2}$$

where b_t is the total tether width, r_w is the radius of the wires composing the tether (see Fig. 2), and V_t the actual tether voltage.

Assuming a constant thrust per unit length, the total brake force modulus F becomes

$$F = L_t\, K\, m_i\, n_0\, v_0^2 \sqrt{\frac{\varepsilon_0\, V_r}{e\, n_0}} \exp\left(-\frac{m_i\, v_0^2}{2\, e\, V_r}\right) \tag{3}$$

where L_t is the tether length. The brake force expression neglects the effects of Earth's magnetic field. This is a reasonable simplification, since the magnetic field reduces the (electrostatic) drag only if the tether current is high and the component along the tether axis of the magnetic inductance vector is large [4]. Therefore, when the spacecraft orbital inclination is small, the effects of the magnetic field can be neglected since, in this case, the magnetic field lines are nearly orthogonal to the orbital plane. However, even for medium-high orbital inclinations, the magnetic inductance vector is aligned with the tether axis only for small time intervals (corresponding to high latitudes).

All of the variables in Eqs. (2)–(3) are, in general, functions of time (through solar activity) and spacecraft position (i.e. altitude, right ascension, and declination), which makes the plasma brake simulation a rather complex problem. It is therefore advisable to lower the number of variables involved in Eqs. (2)–(3) by means of some preliminary considerations in order to simplify the analysis and reduce the simulation costs. To this end, consider a spacecraft orbiting a highly-populated near-circular LEO, i.e. an orbit with an altitude in the range 300km − 1000km. In this case, the dominant species in the ionosphere is the atomic oxygen, with an atomic mass $m_i = 16$u, see Fig. 3 To a first order approximation,

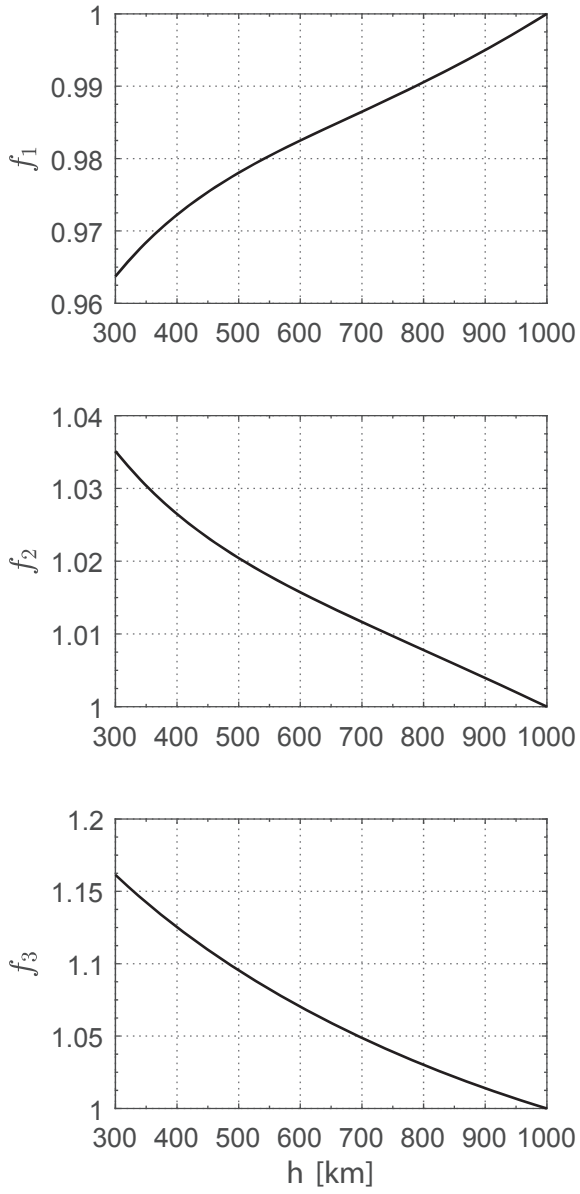

Fig. 4. Variation of the f_i terms as functions of the altitude (reference value at 1000km) for a mean solar activity.

the velocity of ions (relative to the tether) is considered constant along the tether and equal to the speed at which the spacecraft orbits around the Earth. Finally, a mean solar activity is considered for the rest of the paper, which implies a mean value of the plasma brake-induced drag. As a result, the number of free parameters in Eqs. (2)–(3) reduces to four, that is, the two design variables $\{V_t, L_t\}$, the bulk number density of ions n_0, and the spacecraft altitude h, since $v_0 = v_0(h)$.

The values of n_0 can be estimated with different degrees of accuracy [25–27] using either the geopotential model or the International Reference Ionosphere (IRI) model. The former is simple and analytical, so it can be used to derive an approximate plasma brake performance model, while the latter is complex and accurate, and is used to validate the (analytical) results.

The resulting profile of n_0 is determined by the following expression [25–27].

$$n_0 = \tilde{n}_0 \exp\left\{-\frac{m_i\, g_0\, R_\oplus^2}{2\, k_B\, T}\left[\frac{h}{(R_\oplus + h)^2} - \frac{\tilde{h}}{(R_\oplus + \tilde{h})^2}\right]\right\} \tag{4}$$

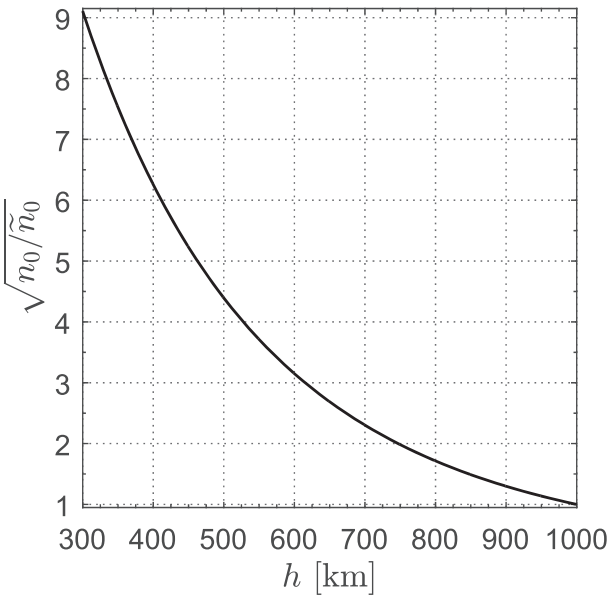

Fig. 5. Normalized ion density as a function of altitude (reference value at 1000km) for a mean solar activity.

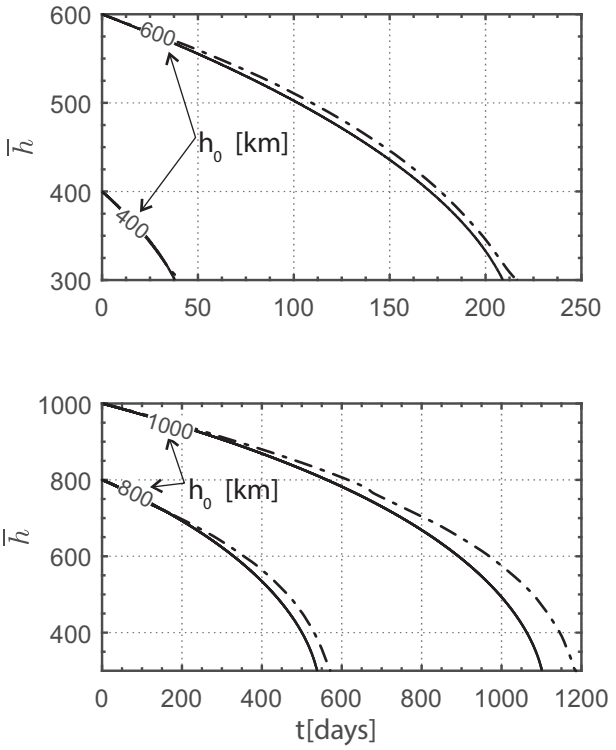

Fig. 6. Mean altitude time-variation with approximate (solid line) and IRI-based (dash-dot line) models for different initial altitudes (when $h_0 = 400$km the two profiles are nearly identical). A mean solar activity is assumed.

where the tilde symbols identify quantities measured at a reference altitude $\tilde{h}$. In Eq. (4), h is the spacecraft altitude, k_B is the Boltzmann constant, g_0 is the standard gravity, $R_\oplus$ is the Earth's mean radius, and T is the temperature of ions, assumed equal to that of electrons and neutral particles (due to thermal equilibrium considerations), with a typical value of 1011.5K for mean solar activity [25,26]. From the previous simplifications, the only remaining variable in Eq. (4) is the spacecraft altitude h.

In analogy with Eq. (4) and assuming a constant tether voltage V_t (constrained by onboard power availability and field emission current issues), Eq. (3) is normalized with a thrust reference value $\tilde{F}$ as

$$F = \tilde{F}\sqrt{\frac{n_0}{\tilde{n}_0}}\left(\frac{v_0}{\tilde{v}_0}\right)^2 f_1(v_0) f_2(n_0, v_0) f_3(n_0) \tag{5}$$

where

$$f_1(v_0) \triangleq \left(\frac{\varepsilon_0 |V_t|}{e\, b_t\, r_w}\right)^{-\frac{m_i}{4\, e|V_t|}\left(v_0^2 - \tilde{v}_0^2\right)} \tag{6}$$

$$f_2(n_0, v_0) \triangleq n_0^{\frac{m_i\, v_0^2}{4\, e\, |V_t|}}\, \tilde{n}_0^{-\frac{m_i\, \tilde{v}_0^2}{4\, e\, |V_t|}} \tag{7}$$

$$f_3(n_0) \triangleq \left\{ \frac{\left[\ln\left(\frac{\varepsilon_0 |V_t|}{e\, b_t\, r_w}\right)\right]^{\frac{e}{2\,\varepsilon_0 |V_t|}} - [\ln(n_0)]^{\frac{e}{2\,\varepsilon_0 |V_t|}}}{\left[\ln\left(\frac{\varepsilon_0 |V_t|}{e\, b_t\, r_w}\right)\right]^{\frac{e}{2\,\varepsilon_0 |V_t|}} - [\ln(\tilde{n}_0)]^{\frac{e}{2\,\varepsilon_0 |V_t|}}} \right\}^{-\frac{1}{2}} \tag{8}$$

An additional simplification of the mathematical model may be obtained by estimating the order of magnitudes of the different terms involved in Eq. (5). For nearly-circular LEOs, the variation range of velocity is related to the orbital altitude only. Since $300 \leq h \leq 1000$km, it is found that

$$0.91 \leq \frac{v_0^2}{\tilde{v}_0^2} \simeq \frac{\tilde{h} + R_\oplus}{h + R_\oplus} \leq 1.10 \tag{9}$$

and the approximation $(v_0^2/\tilde{v}_0^2) \simeq 1$ is reasonable. Moreover, taking $\tilde{h} \triangleq 1000$km as the reference altitude value, it is possible to evaluate the variation of f_1, f_2 and f_3 as functions of h. As shown in Fig. 4, f_1 and f_2 take values close to 1 and show very little and opposite variations in the considered range. The f_3 term, calculated with Eq. (8), is also sufficiently close to 1. Therefore, the simplification $f_1(v_0)\, f_2(n_0, v_0)\, f_3(n_0) \simeq 1$ will be used in the following analysis.

The dominant term in Eq. (5) is then the bulk number density n_0, which is strongly variable with the altitude, see Fig. 5.

Accordingly, a compact version of Eq. (5) can be written as

$$F \simeq \tilde{F}\sqrt{\frac{n_0}{\tilde{n}_0}} \tag{10}$$

Substituting Eq. (4) into Eq. (10), the analytical expression of the plasma brake force as a function of the spacecraft altitude is

$$F = \tilde{F}\exp\left\{ -\frac{m_i\, g_0\, R_\oplus^2}{4\, k_B\, T}\left[\frac{h}{(R_\oplus + h)^2} - \frac{\tilde{h}}{(R_\oplus + \tilde{h})^2}\right]\right\} \tag{11}$$

where the reference value $\tilde{F}$ comes from Eq. (3) with $n_0 = \tilde{n}_0$.

2.1. Model validation

The previous mathematical model is now validated by simulation using a single negatively-charged tether, released by a spacecraft with a total mass $m_{SC} = 40$kg (including the tether and the tip mass) and a frontal area $A = 0.03\text{m}^2$. For example, the ESTCube-1 satellite [18] was equipped with a 10m-long tether with a tip mass of 1.2g, corresponding to about one hundredth of the spacecraft total mass. Typical values (with current technology level [4,15]) for tether length, width, and wire radius are $L_t = 1$km, $b_t = 2$cm, and $r_w \geq 25\mu$m, respectively. From Eqs. (2)–(3), it can be shown that the maximum thrust corresponds to the minimum value of r_w and, therefore, the wire radius is set equal to 25μm. Every simulation is stopped when the mean altitude $\overline{h} = a - R_\oplus$ (being a the semimajor axis of the osculating orbit) reaches 300km, i.e. when the effect of atmospheric drag becomes a dominant term.

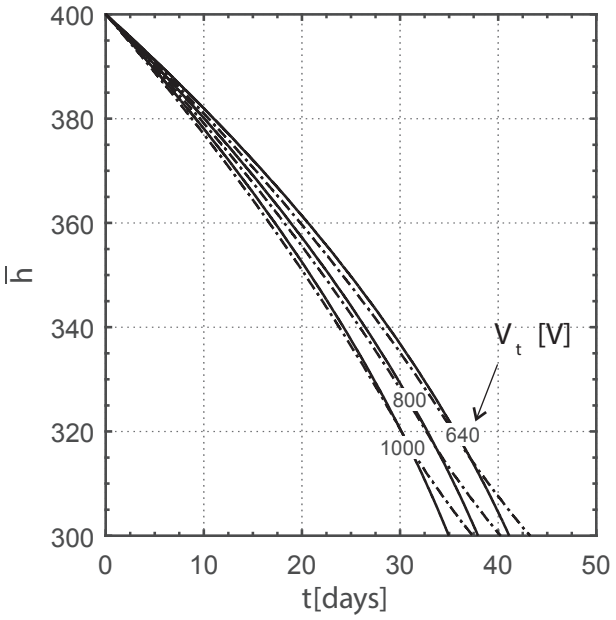

Fig. 7. Mean altitude time-variation with analytical (solid line) and IRI-based (dash-dot line) models for different tether voltages ($h_0 = 400$km). A mean solar activity is assumed.

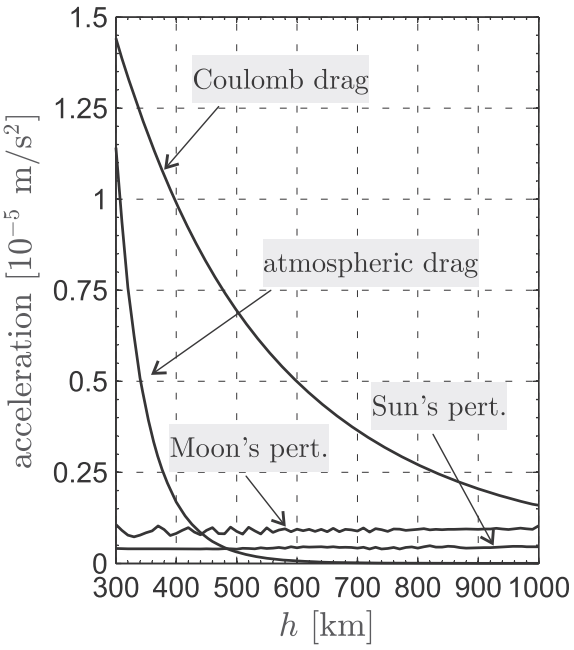

Fig. 8. Perturbative accelerations acting on a 40kg-spacecraft with $L_t = 1$km during the deorbiting phase as a function of the altitude h.

The accuracy of the approximate model has been verified by comparing the results with those obtained using a IRI-based numerical model in which the actual spacecraft state is calculated through numerical integration of the equations of motion (including main orbital perturbations). In particular, the mean molecular mass of ions and the bulk number density are evaluated by interpolating the IRI tabular data (for a mean solar activity) as functions of the altitude-longitude and selecting a mean value for the latitude, in analogy with MSIS-E-90 atmospheric model [25,26]. As the magnetic field effects are neglected, the orbital inclination is set equal to zero without any loss of generality. In addition to the Coulomb drag, the simulations take into account the Earth's oblateness (up to the 4th zonal harmonic), the luni-solar gravitational perturbations, and the atmospheric drag (where the atmospheric density is calculated with the MSIS-E-90 model).

Fig. 6 shows the time-variation of $\overline{h}$ in the osculating orbit as a function of the initial spacecraft altitude $h_0 \in \{400, 600, 800, 1000\}$km, comparing the approximate method with the IRI-based model. The negative tether voltage is set equal to its maximum allowable value, to maximize the magnitude of the plasma brake-induced drag, see Eq. (3). In particular $V_t = 800$V, a value consistent with the specifications [21] of satellite Aalto-1. For each initial altitude h_0, the approximate model is able of estimating the deorbiting time with a percentage error less than 6% when compared to that calculated with the IRI-based model. Numerical simulations show that such a small error is a good compromise between system complexity and simulation costs, since it is obtained with a reduction in computational time of about two order of magnitudes. Fig. 7 shows the mean altitude time history corresponding to an initial altitude of 400km, with different tether voltages $|V_t| \in \{640, 800, 1000\}$V. Note that the relative errors of the approximate method with respect to the results from the complete model are smaller than 7%.

3. Mission application

The previous approximate thrust model is useful for simulating a number of potential mission scenarios. A typical application of such a propulsive concept is a deorbiting strategy for a LEO satellite, in which the plasma brake propulsive acceleration slows down the spacecraft velocity and lowers its orbital perigee until the vehicle reaches the most dense atmospheric layers where the aerodynamic drag is sufficient to complete the deorbiting phase in a small time interval. In fact, the problem of space debris has become a substantial concern for future space missions due to the high number of flying objects in LEOs. Note that, according to international guidelines, the residual orbit life of an out-of-order satellite should be less than 25 years [28,29].

3.1. Mission time estimate

The deorbiting performance of a plasma brake system is first investigated using a spacecraft (orbiting an equatorial LEO) equipped with a tether having $b_t = 2$cm and $r_w = 25\mu$m [4]. Based on statistical data [30], the spacecraft mass distribution in LEO has two peak values centered at 40kg or 690kg. To evaluate the plasma brake performance with reasonable computational times, the lower peak value $m_{SC} = 40$kg is selected, which includes the tether and the tip mass. The plasma brake force is estimated with the previous analytical approximate model, while the perturbative forces considered in the simulation are the Earth's oblateness up to the 4th zonal harmonic, the luni-solar effects, and the atmospheric drag. The latter requires the introduction of a ballistic coefficient c_b, defined as

$$c_b = \frac{m_{SC}}{\sum_i (C_D\, A)_i} \tag{12}$$

where the subscript i indicates the generic part of the spacecraft (body, tether, and tip mass) and C_D is the corresponding drag coefficient. The denominator of Eq. (12) is calculated with the following relations, based on Aalto-1 satellite data [20].

$$C_D = \begin{cases} 2.00 & \text{(sphere)} \\ 2.65 & \text{(cylinder)} \end{cases}$$
$$A = \begin{cases} 0.2\text{m}^2 & \text{for the spacecraft body} \\ 2\, r_w\, L_t\, k_t & \text{for the tether} \end{cases} \tag{13}$$

where $k_t = 4.3$ is a factor that accounts for the multiple wires composing the tethers [1]. Note that the atmospheric drag contribution of the tip mass is neglected (this is both a simplifying and a conservative assumption).

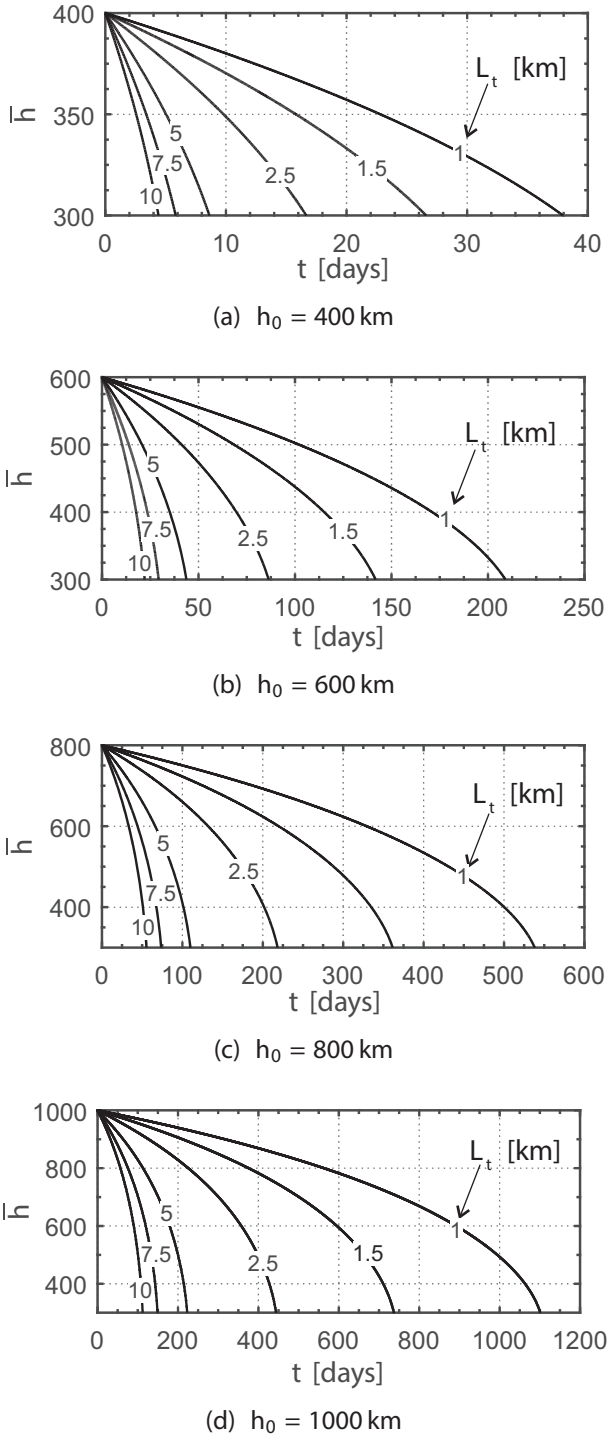

Fig. 9. Approximate deorbiting profiles as functions of time for different tether lengths and initial altitudes. A mean solar activity is assumed.

A comparison among the different accelerations acting on a deorbiting spacecraft (with the Coulomb drag calculated assuming $L_t = 1$km) is shown in Fig. 8, where the magnitude of the perturbation accelerations is plotted as a function of the spacecraft altitude h. The contribution due to the Earth's oblateness is from 3 to 4 order of magnitudes greater than the other effects, but it does not directly affect the orbital altitude and, as such, it has a negligible effect on the deorbiting profile (therefore it is not included in Fig. 8). The luni-solar effect has a small magnitude at any spacecraft altitude, and its influence on the orbital semimajor axis is not significant [31]. Hence, the deorbiting effect is essentially governed by the action of the Coulomb drag and the atmospheric drag, with the former representing the main contribution within the whole altitude range. Note that the atmospheric drag is comparable to the plasma brake-induced drag as long as $h < 350$km, while it becomes negligible when $h > 400$km. These considerations are in accordance with the results presented in Ref. [32], where a Electrodynamic Tether-enabled deorbiting maneuver is studied.

The simulated deorbiting profiles are plotted in Fig. 9 for different tether lengths $L_t \in [1, 10]$km and initial altitudes $h_0 \in \{400, 600, 800, 1000\}$km. Note that, for $h_0 = 1000$km, the final deorbiting time decreases almost linearly with $1/L_t$, as is predicted from Eq. (3), but the same trend is not so clear for lower initial altitudes. The reason for this behavior is that at high altitudes the plasma brake force represents the dominant "perturbative" acceleration, and therefore it strongly influences the deorbiting time (see Fig. 8). At lower altitudes the contribution of the atmospheric drag is increased, leading to a complex coupling between aerodynamic and plasma brake accelerations.

The estimated decaying times are in accordance with the international guidelines [28], suggesting that the plasma brake technology may be a potential option capable of providing sufficiently fast satellite deorbiting for LEO applications. The use of plasma brake technology implies a slower decaying rate when compared to more conventional deorbiting strategies (based on chemical or electrical thrusters), but a significant mass saving is possible with the propellantless option, as is now discussed.

3.2. Comparison with chemical and electric thrusters

The performance of a plasma brake system can be quantified in terms of payload mass fraction. To this end, the total decaying time for a given mission scenario is maintained constant. The mean drag acceleration acting on the spacecraft is therefore fixed, while the tether length increases linearly with the spacecraft total mass, see Eq. (3). The resulting plasma brake payload mass fraction λ_{PB} can be calculated as

$$\lambda_{PB} = \frac{m_L}{m_0} = 1 - \frac{L_t\,\sigma_t}{m_0}\left(1 + \frac{\rho_r}{\rho_w\,\eta_r}\right) - \frac{m_{rm}}{m_0} \tag{14}$$

where m_L is the payload mass, m_0 is the spacecraft initial mass, $m_{rm} = 0.326$kg is the tether reel mechanism mass estimated using the data from Aalto-1 spacecraft [21], $\sigma_t = 3.3772{\cdot}10^{-5}$kg/m is the tether structural coefficient (corresponding to the previously assumed values of r_w and b_t), $\rho_w = 4000\text{kg/m}^3$ is the wire density (made of an aluminium-copper alloy), $\rho_r = 500\text{kg/m}^3$ is the estimated mass density of the reel structure, and $\eta_r = 0.3$ is the packaging factor of the reeled tether. For a more in depth discussion about the terms involved in Eq. (14) and the mathematical model for their estimation, the interested reader is referred to Ref. [33].

Plasma brake technology may be compared to a more conventional deorbiting system based on a chemical or an electrical thruster. The corresponding payload mass fraction λ_C may be expressed as

$$\lambda_C = \frac{1 - f_P - \sigma_S}{1 - \sigma_S} \tag{15}$$

where σ_S is the structural coefficient and f_P is the propellant mass fraction calculated with the Tsiolkovsky equation. An estimate of the structural coefficients and propellant mass fractions for a chemical or an electric thruster requires some information about the propulsion system characteristics. The reference commercial thrusters chosen for comparative purposes are the Safran 20N hydrazine thruster, and the Sitael HT400 Hall Effect Thruster, whose characteristics are summarized in Table 1. The tankage fraction is estimated for both thruster with a typical state-of-the-art value of 0.02.

The payload mass fraction that can be saved with a plasma brake system can be evaluated as follows

Table 1
Characteristics of the reference propulsion systems.

	Safran 20N hydrazine thruster	Sitael HT400 HET
Thruster mass	0.65kg	0.9kg
Specific impulse	230s	1850s

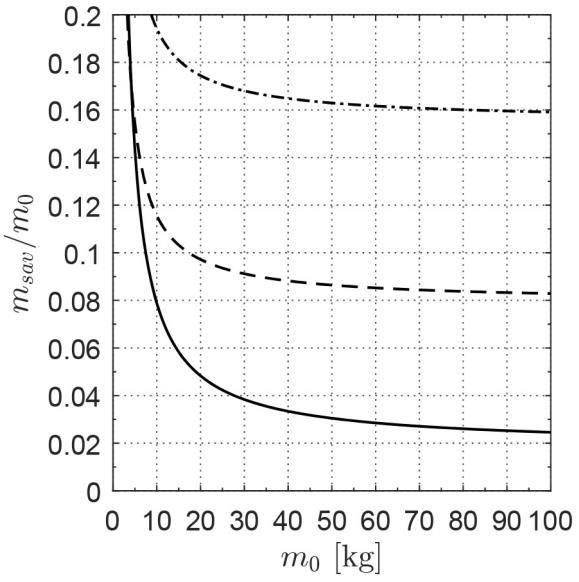

Fig. 10. Fraction of saved mass with plasma brake ($L_t = 1$km) compared to chemical propulsion fast deorbiting (dash-dot line), chemical propulsion slow deorbiting (dashed line), and electric propulsion deorbiting (solid line) for $h_0 = 1000$km.

$$m_{sav} = m_0\left(1 - \frac{\lambda_C}{\lambda_{PB}}\right) \tag{16}$$

which is plotted in Fig. 10 as a function of the total initial mass for different deorbiting strategies. In particular, three possible strategies are considered: 1) a Hohmann transfer from h_0 to the final altitude of 300km (fast deorbiting with chemical propulsion), 2) an impulsive manoeuvre that lowers the perigee altitude to 300km (slow deorbiting with chemical propulsion), and 3) a low thrust transfer from h_0 to 300km (deorbiting with electric propulsion). The payload mass fraction that can be saved is substantial, especially for small or medium-sized spacecraft. In addition, it can be shown that an increase in the tether length has a minor effect on the value of the payload mass fraction. For example, assuming a tether length of 5km, a spacecraft mass of 50kg and a slow deorbiting strategy with chemical propulsion, the decrease in m_{sav}/m_0 is about 0.44% only when compared to a tether length of 1km. This is a very interesting result since the tether length has a substantial effect on the decaying time, as shown in Fig. 9.

4. Conclusions

An approximate method for estimating the plasma brake performance has been discussed. Such a mathematical model is based on the introduction of suitable simplifying assumptions in the calculation of the plasma brake force as a function of the spacecraft altitude and the other system design parameters.

The analytical model is validated by comparison with the results obtained with numerical simulations (based on the integration of the spacecraft equations of motion) that take into account the actual variation of the ionosphere properties. It is shown that the relative percentage errors of the approximate results are below 7%, when both a varying tether voltage and different initial altitudes are considered, with a substantial decrease of computational times.

The simplified model has been used to evaluate the plasma brake performance in some exemplary cases, such as the deorbiting mission of a small spacecraft initially placed in a low Earth orbit. The obtained results show that the estimated deorbiting times are in good agreement with the international guidelines, and the plasma brake concept may be a competitive option compared to more conventional propulsion systems in terms of required mass fraction (for a given mission time). In this sense, the obtained results are encouraging for the development of the plasma brake technology.

References

[1] P. Janhunen, On the feasibility of a negative polarity electric sail, Ann. Geophys. 27 (4) (2009) 1439–1447, https://doi.org/10.5194/angeo-27-1439-2009.
[2] P. Janhunen, Electrostatic plasma brake for deorbiting a satellite, J. Propul. Power 26 (2) (2010) 370–372, https://doi.org/10.2514/1.47537.
[3] P. Janhunen, Coulomb drag devices: electric solar wind sail propulsion and ionospheric deorbiting, in: Space Propulsion 2014, Space Propulsion, 2014. Köln, Germany, 2014, paper SP2014_2969331, Session 80.
[4] P. Janhunen, Simulation study of the plasma-brake effect, Ann. Geophys. 32 (2014) 1207–1216, https://doi.org/10.5194/angeo-32-1207-2014.
[5] P. Janhunen, Electric sail for spacecraft propulsion, J. Propul. Power 20 (4) (2004) 763–764, https://doi.org/10.2514/1.8580.
[6] P. Janhunen, P.K. Toivanen, J. Polkko, et al., Electric solar wind sail: toward test missions, Rev. Sci. Instrum. 81 (11) (2010), https://doi.org/10.1063/1.3514548, 111301–1–11301–11.
[7] G. Mengali, A.A. Quarta, P. Janhunen, Electric sail performance analysis, J. Spacecraft Rockets 45 (1) (2008) 122–129, https://doi.org/10.2514/1.31769.
[8] L. Niccolai, A.A. Quarta, G. Mengali, Electric sail-based displaced orbits with refined thrust model, Proc. Inst. Mech. Eng. Part G: J. Aero. Eng. https://doi.org/10.1177/0954410016679195. (In press).
[9] L. Niccolai, A.A. Quarta, G. Mengali, Electric sail elliptic displaced orbits with advanced thrust model, Acta Astronaut. 138 (2017) 431–440, https://doi.org/10.1016/j.actaastro.2016.10.036.
[10] A.A. Quarta, G. Mengali, Electric sail mission analysis for outer solar system exploration, J. Guid. Contr. Dynam. 33 (3) (2010) 740–755, https://doi.org/10.2514/1.47006.
[11] K. Yamaguchi, H. Yamakawa, Electric solar wind sail kinetic energy impactor for near earth asteroid deflection mission, J. Astronaut. Sci. 63 (1) (2016) 1–22, https://doi.org/10.1007/s40295-015-0081-x.
[12] G. Mengali, A.A. Quarta, Optimal nodal flyby with near-earth asteroid using electric sail, Acta Astronaut. 104 (2) (2014) 450–457, https://doi.org/10.1016/j.actaastro.2014.02.012.
[13] A. A. Quarta, G. Mengali, P. Janhunen, Electric sail for a near-earth asteroid sample return mission: case 1998 KY26, J. Aero. Eng. 27(6), doi: 10.1061/(ASCE)AS.1943-5525.0000285.
[14] R.L. Forward, Failsafe multistrand tether structures for space propulsion, in: 28th Joint Propulsion Conference and Exhibit, AIAA, Nashvile, Tennessee, USA, 1992.
[15] H. Seppänen, T. Rauhala, S. Kiprich, J. Ukkonen, M. Simonsson, R. Kurppa, P. Janhunen, E. Hæggstrom, One kilometer (1 km) electric solar wind sail tether produced automatically, Rev. Sci. Instrum. 84(9), doi: 10.1063/1.4819795.
[16] H. Seppänen, S. Kiprich, R. Kurppa, P. Janhunen, E. Hæggström, Wire-to-wire bonding of μm-diameter aluminum wires for the electric solar wind sail, Microelectron. Eng. 88 (11) (2011) 3267–3269, https://doi.org/10.1016/j.mee.2011.07.002.
[17] T. Rauhala, H. Seppänen, J. Ukkonen, S. Kiprich, G. Maconi, P. Janhunen, E. Hæggström, Automatic 4-wire heytether production for the electric solar wind sail, in: Proc. International Microelectronics Assembly and Packing Society Topical Workshop and Tabletop Exhibition on Wire Bonding, San Jose, California, 2013.
[18] S. Latt, A. Slavinskis, E. Ilbis, et al., Estcube-1 nanosatellite for electric solar wind sail in-orbit technology demonstration, Proc. Est. Acad. Sci. 63 (2S) (2014) 200–209, https://doi.org/10.3176/proc.2014.2S.01.
[19] A. Slavinskis, M. Pajusalu, H. Kuuste, et al., Estcube-1 in-orbit experience and lessons learned, IEEE Aero. Electron. Syst. Mag. 30 (8) (2015) 12–22, https://doi.org/10.1109/MAES.2015.150034.
[20] A. Kestila, T. Tikka, P. Peitso, et al., Aalto-1 nanosatellite - technical description and mission objectives, Geoscientific Instrumentation, Methods and Data Systems 2 (2013) 121–130, https://doi.org/10.5194/gi-2-121-2013.
[21] O. Khurshid, T. Tikka, J. Praks, M. Hallikainen, Accomodating the plasma brake experiment on-board the Aalto-1 satellite, Proc. Est. Acad. Sci. 63 (2S) (2014) 258–266, https://doi.org/10.3176/proc.2014.2S.07.
[22] P. Janhunen, P. Toivanen, J. Envall, A. Slavinskis, Using charges tether coulomb drag: E-sail and plasma brake, in: 5th International Conference on Tethers in Space, Ann Arbor, Michigan, USA, 2016.
[23] U. Kvell, D. Di Cara, P. Janhunen, M. Noorma, J.A. Gonzalez del Amo, Deorbiting strategies: comparison between electrostatic plasma brake and conventional propulsion, in: 47th AIAA/ASME/SAE/ASEE Joint Propulsion Conference & Exhibit, AIAA, ASME, SAE, ASEE, San Diego, California, USA, 2011.
[24] P. Janhunen, Increased electric sail thrust through removal of trapped shielding electrons by orbit chaotisation due to spacecraft body, Ann. Geophys. 27 (8) (2009) 3089–3100, https://doi.org/10.5194/angeo-27-3089-2009.

[25] A.E. Hedin, J.E. Salah, J.V. Evans, et al., A global thermospheric model based on mass spectrometer and incoherent scatter data 1. N2 density and temperature, J. Geophys. Res. 82 (16) (1977) 2139–2147, https://doi.org/10.1029/JA082i016p02139.
[26] A.E. Hedin, C.A. Reber, G.P. Newton, N.W. Spencer, H.C. Brinton, H.G. Mayr, W.E. Potter, A global thermospheric model based on mass spectrometer and incoherent scatter data 2. composition, J. Geophys. Res. 82 (16) (1977) 2148–2156, https://doi.org/10.1029/JA082i016p02148.
[27] D. Bilitza, The international reference ionosphere - status 2013, Adv. Space Res. 55 (8) (2015) 1914–1927, https://doi.org/10.1016/j.asr.2014.07.032.
[28] F. Schäfer, M. Lambert, E. Christiansen, S. Kibe, H. Stokes, H.G. Reimerdes, S.A. Meshcheryakov, F. Angrilli, H. Zengyao, The inter-agency space debris coordination committee (IADC) protection manual, in: 4th European Conference on Space Debris, European Space Agency (ESA), Darmstadt, Germany, 2005.
[29] M. Yakovlev, The "IADC space debris mitigation guidelines" and support document, in: 4th European Conference on Space Debris, European Space Agency (ESA), Darmstadt, Germany, 2005.
[30] B. Bastida Virgili, H. Krag, Strategies for active removal in LEO, in: 5th European Conference on Space Debris, March 30 – April 2, Darmstadt, Germany, 2009.
[31] G.E. Cook, Luni-solar perturbations of the orbit of an earth satellite, The Geophysical Journal 6 (3) (1962) 271–291, https://doi.org/10.1111/j.1365-246X.1962.tb00351.x.
[32] R. Zhong, Z.H. Zhu, Dynamics of nanosatellite deorbit by bare electrodynamic tether in low earth orbit, J. Spacecraft Rockets 50 (3) (2013) 691–700, https://doi.org/10.2514/1.A32336.
[33] P. Janhunen, A.A. Quarta, G. Mengali, Electric solar wind sail mass budget model, Geoscientific Instrumentation, Methods and Data Systems 2 (1) (2013) 85–95.